Functional Materials 19, No.4 (2012)

Formation mechanisms and geometry of the crack assemble formed under uniaxial cyclic compression of NaCl single crystals

Yu.I.Boyko, M.A.Volosyuk, V.G.Kononenko

Institute for Scintillation Materials, STC "Institute for Single Crystals", National Academy of Sciences of Ukraine, 60 Lenin Ave., 61001 Kharkiv, Ukraine
V.Karazin Kharkiv National University, 4 Svobody Sqr., 61077 Kharkiv, Ukraine

Received September 5, 2012

Using light-scattering method, the cracks formation was experimentally studied in NaCl single crystals under uniaxial cyclic compression (10^7 N/m^2) during ~10 c at room temperature and following annealing at T = 500°C for ~10 min. The observed cracks were sorted (conventionally, in comparison with wavelength of the light used) into small ones showing the pattern of isotropic scattering, and big ones showing the scattering pattern with sharp maxima. It was established, that both small and big cracks were positioned in {100} planes and formed by Cottrell mechanism. In late stages of deformation, a little quantity of cracks was observed in {110} planes. Among possible mechanisms of the cracks formation, Stroh mechanism is considered as the most probable in our case of small deformations and stress. As the cracks are accumulated, the formation of ordered compact groups of cracks is found which are analogous to ordered groups of solid foreign-phase precipitations under decomposition of supersaturated solid solutions. The volume fraction of small cracks is by two orders of value higher than the volume fraction of big ones. The volume fractions of both kinds of cracks increase with the cycle number, but the big crack volume fraction increases much faster.

Экспериментально исследовано методом светорассеяния образование трещин в монокристаллах NaCl в условиях одноосного циклического сжатия (10^7 Н/м^2) в течение ~10 с при комнатной температуре и последующего отжига при T = 500°C в течение ~10 мин. Наблюдаемые трещины по размерам разделены (условно, по сравнению с длиной волны используемого света) на малые, дающие изотропную картину рассеяния, и крупные, картина рассеяния света которыми содержит резкие максимумы. Установлено, что и малые, и крупные трещины располагаются в плоскостях типа {100} и образуются механизмом Коттрелла. На далеких стадиях деформирования наблюдаются в небольшом количестве трещины в плоскостях типа {110}. Из возможных механизмов их образования в нашем случае (малых деформаций и напряжений) наиболее вероятным представляется механизм Стро. Обнаружено, по мере накопления трещин, образование упорядоченных компактных групп трещин, аналогичных упорядоченным группам твердых инофазных выделений при распаде пересыщенных твердых растворов. Объемная доля малых трещин на два порядка превосходит объемную долю крупных. Объемные доли тех и других растут с номером цикла, но опережающим темпом растет доля крупных трещин.

1. Introduction

The problem of solids strength is very deeply intertwined with a problem of different defects formation in the solid under loading [1] — dislocations, micro-cracks [2], pores, etc., including also statistical ones connected with energy fluctuations. The observed patterns [3–6] can be understood only on the basis of experimental studying and analyzing the evolution of all components of materials defect structure in their inseparable connection. A lot of experimental data have been accumulated also on the evolution of defect structures during deformation [7–10]. However, the question about physical mechanisms of stress relaxation nearby the present and just formed stress local concentrators and related transformation of the defect structure remains practically open. As well, direct investigations are necessary to understand the interconnection of elemental acts of plastic deformation and destruction that demands various measuring instruments.

For transparent objects, such as alkali-halide (AH) single crystals, the technique for studying the defect structure was developed basing on measuring the patterns of light scattering during defect formation [11]. The information on geometry, sizes and arrangement of the defects as scattering centers is obtained from experimental data on spatial distribution of light-scattering intensity [11, 12].

In the present work was aimed at the study of geometry and formation mechanisms of crack assemble in NaCl single crystals under cycling uniaxial compression using the light-scattering method. It was shown experimentally and theoretically that under loading cycling, accumulation of crystalline lattice faults took place [7, 13]. This is connected to the fact that practically always under secondary loading the deformation takes place due to new shears formation [14].

2. Experimental

As the objects of the study optically transparent NaCl single crystals were selected, which are less hygroscopic than KCl and KBr, and more convenient for studying by light-scattering method.

From NaCl single crystals grown by Kyropulos method, the samples in the form of cylinders with axis parallel to crystallographic direction ⟨100⟩ and sizes $d = 8$ mm and $h = 15$ mm were made. The samples were subjected to normalizing annealing at

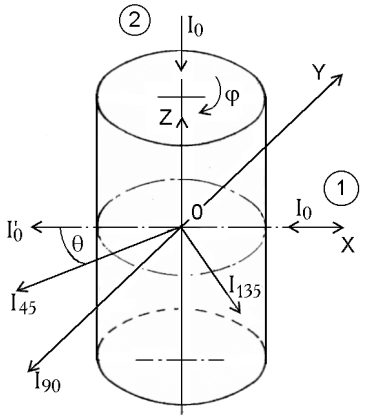

Fig. 1. The scheme for light scattering intensity measurements: a) *1* and *2* are, respectively, lateral and axial lighting the sample; I_0, I_0', I_θ are intensities of incident beam, directly passed one, and one scattered at the angle θ, respectively.

$T = 700°$ during $t = 1$ h, after that the light-scattering intensity was measured. The procedure of the experiment consisted in cyclic repeating of deforming and annealing operations followed by the light-scattering intensity measurements after each operation. For each sample, 4–5 cycles in all were performed. The observation results were averaged over a series of 20 samples.

The sample deformation was carried out along the cylinder axis coinciding with ⟨100⟩ type direction at room temperature under stress $\sigma = 10^7 \mathrm{N/m^2}$, and holding under loading for about 10 s. Under this stress, the noticeable variation of the light-scattering pattern was observed already at the first deformation step. Under loading $4 \cdot 10^7 \mathrm{N/m^2}$, the authors of [15] observed the formation of large micro-cracks and large (of an order of 100 μm) globe-shaped assemblages of pores.

Annealing was carried out at $T = 500°\mathrm{C}$ for 10 min in order to somewhat stress relaxation near concentrators, thus, to prevent the formation of visible main cracks [16]. In order to avoid large thermal stress, both heating and cooling of the sample were carried out together with the furnace approximately for 10 min. As the estimations made by the technique [17] and the experimental testing showed, thermo-elastic stress were minimum, and the dislocation density did not increase under such regime of thermal treatment.

The scheme for measurement of scattered light intensity is shown in Fig. 1. Two variants of lighting were used: (1) lateral light-

ing, and (2) axial lighting. The sample could revolve on its axis, thus varying φ angle setting the crystallographic orientation of the crystal within the incident light beam at θ = *const*. The scattered light was registered in *XOY* plane where the incident I_0 and the scattered $I(\theta)$ light beams laid, which is named the scattering plane. The dependence $I(\theta)$ at lateral lighting is named the scattering indicatrix. For spherical particles with size less than incident light wavelength, the indicatrix is mirror-symmetrical relative to *XOZ* plane. As the particle size increases to values comparative or larger than the incident light wavelength, the indicatrix becomes asymmetric — stretched forward (along the incident light beam). This fact is used for determination of the scattering particle sizes, or even the function of the particles size distribution. If the scattering centers are not spherical, the pattern of spatial distribution of the scattering light becomes substantially complicated; therefore, for each specific form of particles, taking into consideration their spatial arrangement and physical properties, the solution of the corresponding direct problem is necessary.

For the case of AH single crystals with FCC lattice, it is expected that the foreign particles appearing in them will have the parallelepiped-like limiting forms (cubes, plates, or rods). In [11], on the base of the direct problem solution for such particles with different ratios of sides and their sizes but with low refraction index relative to the matrix (Rayleigh-Gans approximation), the angle dependences of light-scattering $I(\varphi)$ at θ = *const* for lateral and axis lighting, and $I(\theta)$ at φ = *const* for lateral lighting were calculated by the computer. These allow determinating the particle forms and crystallographic orientations firmly enough by comparing the calculated and experimental dependences. Notice, that in principle this technique can be applied also for transparent crystals of another symmetry providing the direct problem solution for another particle forms.

The sizes of anisomeric particles can be determined by the angle half-widths of corresponding light-scattering maxima; by the ratios of the heights of corresponding maxima $I(\varphi)$ at θ = 45° and θ = 135°; by elongation of the scattering indicatrix, as it was described in [11]. The particle concentration is determined by the light-scattering intensity (I) at θ = 90° from the expression:

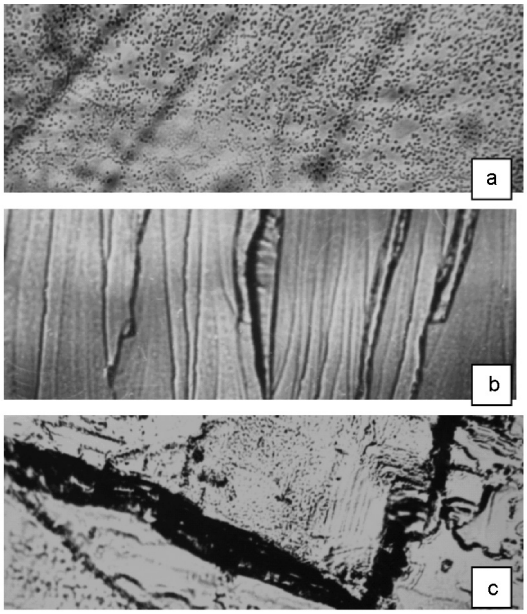

Fig. 2. Micrographs of dislocation structures for NaCl single crystal: a — the initial sample before deformation (×180), b, c — after the third and fifths deformation cycles, (×180).

$$I = 2.9 \cdot 10^{17} N \upsilon^2 \Phi^2(\theta, \alpha_{ik}), \qquad (1)$$

where N, υ are particle concentration and volume, respectively; $\Phi^2(\theta, \alpha_{ik})$ is phase function taking into consideration the phase relations of waves scattered by particle elemental volumes, and determined by the technique given in [11]; α_{ik} is the direction cosine matrix describing the position of the particle proper coordinate system within the laboratory coordinate system (*XOY*). The factor $2.9 \cdot 10^{17}$ takes into account all geometric, physical, and light-, and electrotechnical parameters of the installation, and allows expression of the light-scattering intensity in mV. The light-scattering diagrams $I(\varphi)$ are measured at lateral lighting with settled angles θ = 45°, 90°, 135°, and at axial lighting with θ = 90°.

3. Experimental results

The dislocation structure was studied on special samples cut off the same block of NaCl single crystal which was used also for preparation of cylinder samples for measuring the light-scattering. The samples had a shape of parallelepipeds with 8×8×15 mm^3 sizes and were subjected to temperature — loading treatment using the same technique

as for the samples for light-scattering experiments. In Fig. 2 the dislocation structures are shown for the initial sample (a) and the samples after the third (b) and the fifth (c) cycles. The dislocation density in the initial sample was about $2 \cdot 10^9$ m^{-2}. After the first deformation, the dislocation density increased by a factor about 2–3. After several loading cycles, a lot of solder pads occurred on the crystal cleavages, so the surface looked like a little deformed. Etching the surface resulted in non-contrast pattern, and dislocation structure was almost non-recognized (Fig. 2b and 2c).

Examples of typical angle dependences of light-scattering intensities for the initial sample and the sample after the first, second, and third loading cycles are shown in Fig.3. The scattering pattern for the initial sample (dependence $I(\varphi)$ is isotropic under axial lighting. The scattering indicatrix (dependence $I(\theta)$ under lateral lighting) contains no peaks (smooth curve), but being not Rayleigh one, this is somewhat forward elongated. The scattering particle radius, which is determined by the indicatrix asymmetry, was found to be about 1.2·10–7 m, and their concentration was of the order of 10^{13} m^{-3}. The particle shape was unknown, thus, the size given should be understood as an effective radius of the particles. The similar observations were done in [18] where micro-cracks formation was observed in {100} type planes in KCl single crystals (in the solid samples and in the samples with a solitary pore) under conditions of uniform compression of the crystal. Taking into account these and other observations and also the symmetry of NaCl type crystals, it may be assumed that in the sample under consideration in initial state, also micro-cracks and cubic micro-pores bounded by {100} type planes are responsible for the light scattering.

Already the first deformation of the sample results in appearing the scattering peaks in the scattering diagrams for lateral lighting. Qualitative changes are observed in the indicatrix — the scattering peaks appear in it. The "smooth component" of the scattering indicatrix changes: the indicatrix asymmetry decreases, and the trend to increasing the scattering average intensity appears (Fig. 3). This indicates the fact that in the crystal after the first deformation, new scattering particles occurred which sizes are somewhat lower than for the particles present on the initial sample (the indicatrix asymmetry decreased). It may be assumed that these particles are cracks and micro-pores which are usually observed under such conditions.

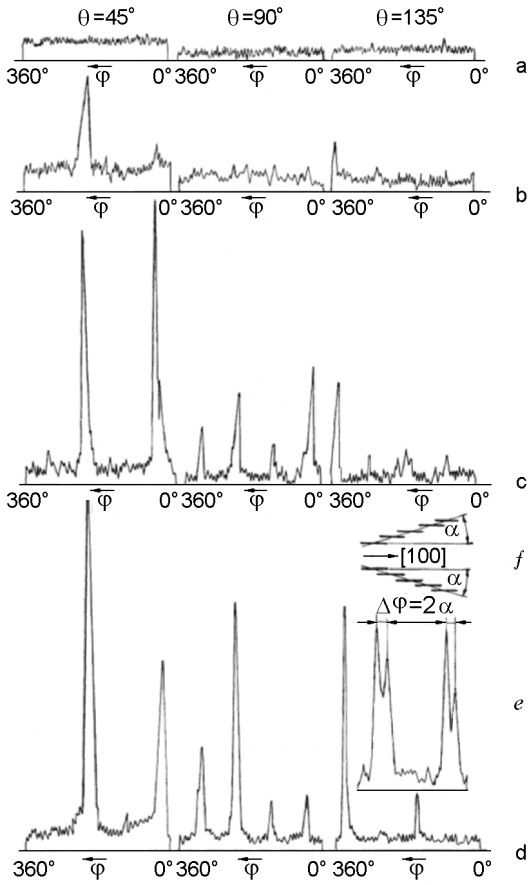

Fig. 3. Examples of scattering diagrams $I(\varphi)$ at fixed angles θ equal to 45°, 90° and 135° under lateral lighting: a — for the initial sample; b, c, d — after the first, the second and the third deformation-annealing cycles, respectively; *e* — example of a split maximum under lateral lighting; *f* — possible scheme of the group. The attenuator positions of the registering device: a — 1 mV, b — 3 mV, c — 10 mV, d — 30 mV.

The $I(\varphi)$ peak symmetry as a rule is absent in the light-scattering diagrams under lateral lighting after the first deformation. Evidently, this is caused by what slip planes from possible ones have taken part in deformation process. Already after the second deformation cycle, most often four scattering peaks are observed in the diagram at θ = 90°, which correspond to the angles φ of crystal rotation: 45°, 135°, 225°, 315° (in initial state, at θ = 0, the direction [100] coincides with the incident beam direction). At the lateral lighting, after two cycles, none of

peaks are observed as a rule in the light scattering diagram $I(\varphi)$.

The indicated arrangement of the peaks in the scattering diagrams at lateral and axial lighting testifies to the fact that in the disperse structure of the sample after deformation, big enough plate particles occurred lying in the planes of {100} type. These particles are, evidently, the cracks. The scattering peaks are not observed from the small cracks, therefore, their orientation is considered to be the same as for the cracks, from which the peaks are observed. Sorting the cracks by sizes into "small" and "big" is rather conventional. That is caused by with the light-scattering method used for their observation: if a particle has a relative size $k_a \cdot a < 1$ ($k_a = 2\pi/\lambda_a$, λ_a is wavelength of the incident light in the medium where the particle is), the scattering diagrams are isotropic, so the particle is considered as small; if particles have the relative size $k_a \cdot a \geq 1$, the scattering intensity peaks appear in the scattering diagrams, so, the particle is considered as big.

The differences between formed cracks sizes are connected with the differences of local conditions for their generation and growth, but their nature, mechanism of generation and growth, the plane of their deposition under the specific experimental conditions are similar (do not depend on the sizes). The formation of some quantity of cubic holes due to vacancy coalescence during plastic deformation and subsequent annealing also must not be ruled out.

After 3–4 cycles of loading and annealing, some scattering peaks are split. After the splitting, the angle distance between the neighboring peaks is from ~10° to 40° ÷ 50°.

4. Discussion

The discussion of the results we begin from the analysis of the data resulted from the scattering indicatrix looking like a smooth curve (without peaks). Such shape of the indicatrix is characteristic for either spherical (isomeric) particles, or, as it was mentioned earlier, for anisomeric particles, if their effective radius $\tilde{a}$ satisfies the condition: $k_a\tilde{a} < 1$ (small particles). In our case, such anisomeric particles are small cracks (as it was mentioned above).

For approximate estimation of the small crack size we apply the following approach. By the indicatrix asymmetry $m = I_{45}/I_{135}$ we determine a certain effective radius $\tilde{a}$ of the particle [11, 12]. Taking into account that the particle scattering intensity averaged over the sample rotation angle φ is determined by the particle volume, we equate the volume of the sphere $(4/3)\pi\tilde{a}^3$ with effective radius $\tilde{a}$ to the volume of a plate $L^2\delta$ (L is the plate width, δ is its thickness). Assuming $(L/\delta) \approx 10 \div 20$, we obtain the estimation of a small crack size: $L \approx 4\tilde{a}$. The crack concentration was determined by the technique proposed in [11].

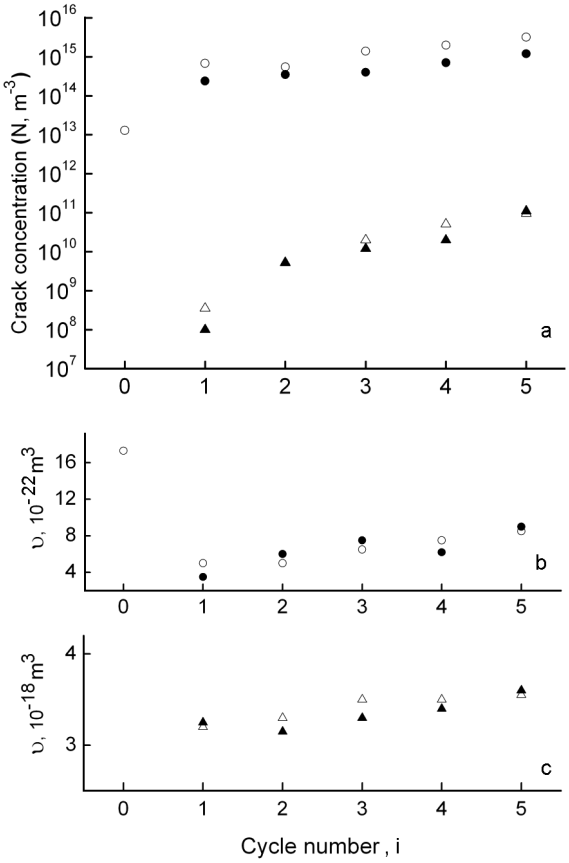

Fig. 4. Dependences of crack concentration ($N\upsilon$) — (*a*), and crack volume (υ) — (*b*, *c*) on the cycle number (*i*): ○● — small cracks, Δ ▲ — big cracks; ○ Δ — after deformation, ● ▲ — after deformation and annealing.

The obtained dependences of concentration (N) and volume (υ) of small cracks on the cycle number (i) are shown in Fig. 4a, b. As it is seen, their volume somewhat decreases in the beginning, and then it shows a trend to increase as the number of cycle (i increases; but as a whole, for all five cycles, the increase of the small crack volume is insignificant. The crack concentration (N) increases with the cycle number, however this trend becomes somewhat slower to the end of the experiment. The observed beginning behavior of the dependence $\upsilon(i)$ is naturally to relate with the fact that in the

initial sample, there were particles of somewhat larger sizes than the new-generated ones. Addition to them of a lot of new cracks of slightly less size decreases a little their observed average size.

Let us clarify, how is justified from the point of view of the energy-force approach the appearance of the cracks with observed sizes, and how can these be stable under low enough average stress applied. According to Griffith criterion, the critical size L^* of a stable crack able to grow is given by the evaluation [16]:

$$L^* = \frac{8G\gamma}{\pi(1-\nu)} \cdot \frac{1}{\sigma^2}, \qquad (2)$$

where G is shear modulus, γ is the specific surface energy, ν is Poisson coefficient, σ is the applied compressive stress. Taking into account that $\gamma \simeq 0.1$ Gb [10] (b is Burgers vector) and substituting the numerical values: $b = 3{\cdot}10^{-10}$ m, $\nu = 0.3$, $G = 1.28{\cdot}10^{10}$ N/m^2, $\sigma = 10^7$ N/m^2, we obtain $L^* \simeq 7{\cdot}10^{-5}$ m. This evaluation indicates that the observed crack size ($L = 4\tilde{a} \simeq 4.8{\cdot}10^{-7}$ m) is by two orders less than the size followed from (2). Such situation occurs practically always [16] and is explained by the fact that the existence of sub-critical size cracks is stabilized not by the applied average stress but by the stress concentration in vertices of dislocation clusters compressed under the applied average stress.

Let us evaluate the possible over-stress value under our conditions using the following model [16]. Let's assume that these stresses occur at the vertex of hindered dislocation clusters. If the cluster is hindered by intersections of the dislocation forest, at the mobile dislocation density ρ the cluster length l will be $l = \rho^{-1/2}$. The dislocation number which can be supported in the cluster by the applied stress σ is determined according to [16] as

$$N = \frac{\pi(1-\nu)l\sigma}{Gb}. \qquad (3)$$

The stress $\tilde{\sigma}$ near the cluster vertex, where $x - l/2 < l/2$, is

$$\tilde{\sigma} = \sigma \cdot \left(\frac{l}{x - l/2}\right)^{1/2}. \qquad (4)$$

Within continual approximation, this formula is valid for the distances more than (x') between the head dislocations in the cluster which, in turn, is of the order of value $x' = l/(2N)$. Substituting in (4) instead of $(x - l/2)$ its limiting value $x' = l/(2N)$ and taking into consideration that in our case $\rho \simeq 6{\cdot}10^9$ m^{-2}, we obtain the value for the over-stress at the cluster vertex: $\tilde{\sigma}/\sigma \simeq 13$. Substituting in (2) the value ($\tilde{\sigma}$) instead of (σ), we obtain for ($\tilde{L}^*$) the value $8{\cdot}10^{-7}$ m. As it is seen, the value ($\tilde{L}^*$) is close to the size of the observed cracks $L \simeq 4.8{\cdot}10^{-7}$ m. Hence, it may be assumed that the crack formation model accepted as the base for the evaluation is quite real, and the cracks observed should be stable (as it is observed experimentally). This is even more justified, taking into account that in ionic crystals of NaCl type the planes {100} being isolated have significantly lower surface energy (γ) than the generally accepted in estimations average value 0.1 Gb. For example, the ratio $(\gamma_{(110)}/\gamma_{(100)}) \approx 2.7$ is known for NaCl. This fact substantially facilitates the generation of cracks positioned just in the {100} planes.

Now, let us discuss the results of experimental observations for big cracks responsible for the peaks in the scattering diagrams. As it was mentioned above, we concluded that the scattering particles having the plate-like shape are positioned in {100} planes. Taking into consideration the anisotropy of the surface energy in NaCl type single crystals as well as its minimum value for {100} planes, the result obtained seems logical. In the mentioned crack arrangement, also the information on the most probable mechanism for their formation is laid. That may be Cottrell mechanism [16] which consists in that in the places of the slipband intersections due to dislocation reactions like $(a/2)[101] + (a/2)[\bar{1}01] \rightleftarrows a[001]$, so called "sitting" dislocations are formed (unable to move). Burgers vector and the line of such 'sitting' dislocation are in the planes of (001) type, while the possible slip planes are {110} and directions ⟨110⟩. Elastic stress from such dislocation walls can relax due to opening the micro-cracks in {100} planes. The similar picture was observed earlier in the experiments on healing the isolated holes by dislocation mechanism under crystal hydrostatic compression. Micro- and macro-cracks in {100} planes were formed in the crystal plastic deformation area joining the pore [18].

The half-width of the big cracks was determined by measuring the angle full width

at half maximum for corresponding scattering maxima using the plots from [11]. It was assumed that the function particle distribution by sizes is Gaussian with dispersion value 0.5. The plate thickness was also determined by the technique proposed in [11]. The particle concentration was determined by Eq.(1) and $\Phi(\theta, \alpha_{ik})$ data taken from [11].

In Fig. 4a, c, the dependences of concentration (N) and big cracks volume (υ) on the cycle number (i) are shown after deformation and after annealing. As it is seen, the volume increase of both big and small cracks is insignificant. The big cracks concentration rises with the cycle number much faster than for the small ones but also shows a trend to slowing.

The dependences of small and big cracks volume fraction ($N\upsilon$) variation on the cycle number are shown in Fig. 5. As it is seen, the volume fractions of both types of cracks increase with the cycle number, but the big cracks fraction increases faster. This is obviously connected with that the big cracks have certainly over-critical size; therefore, these display much lower tendency to closing after loading removing, thus being accumulated both by quantity and by total volume from one cycle to another. The total relative volume of cracks in the crystal is represented as almost a whole by small cracks, and this increases during the loading cycling by about two orders of value.

In the late cycles of deformation, the effect of splitting into two closely positioned peaks is observed for some scattering peaks (Fig. 3e). The similar scattering peak splitting was observed as well in [19] during studying the solid solution decomposition in KCl + Ba system. Also in [19] the ordered groups of $BaCl_2$ precipitations were observed by electron microscopy. Schematically, the conversion of the scattering pattern from the scattering by solitary chaotically distributed parallel plates to the scattering by a compact group of closely arranged plates may be represent as follows. The ordered group shown schematically in Fig. 3f due to interferential addition of waves scattered by each particle of the group causes a maximum on the scattering diagram as a solitary particle with its deposition plane (habitus) forming the angle (α) with {100} plane. As the group may be constructed in two mirror-symmetric directions relative to the deposition plane {100} of individual particle, the habitus of the group may constitute the angle ($\pm\alpha$) with {100}

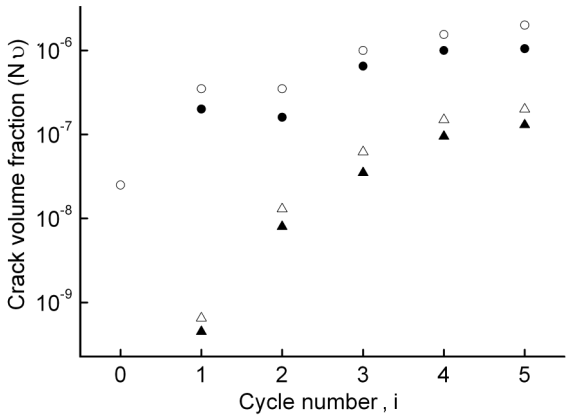

Fig. 5. Dependences of cracks volume fraction ($N\upsilon$) *on the cycle number (i):* ❍ ● — small cracks, Δ ▲ — big cracks; ❍ Δ — after deformation, ●, ▲ — after deformation and annealing.

type plane. This results in splitting the maximum into two maxima shifted relative one another over the crystal turning angle (φ) by the value $\Delta\varphi = 2\alpha$ (see Fig. 3f). Taking into consideration the results of [19] it can be assumed that in our case, the formation of compact ordered groups of cracks is also a consequence of total elastic energy minimization for the crack system including concentration over-stress and mutual arrangement of cracks in the group. In [20] the similar step-wise arrangement of cracks was observed in intermetallide Ti_3Al.

The small cracks have the size close to critical value. They do not close down (at any case, completely) in the existing stress field mainly due to plastic deformation in the mouths. Therefore they are able to open under loading and partially close down after its removing. Additionally, small cracks, displaying none individual scattering anisotropy, are able also to form groups with the same geometry and on account of the same physical causes that bigger particles, thus contributing into intensity of the split scattering maxima.

Along with scattering maxima from cracks lying in the planes {100}, sometimes in late stages of deformation the scattering peaks occur positioned at the angles $\varphi = 0°$, 90°, 180°, 270° under lateral lighting the sample. Also the scattering maxima are observed positioned at the same angles $\varphi = 0°$, 90°, 180°, 270° but under axial lighting. Such configuration of the maxima is caused by cracks lying in {110} planes. These observations are not regular; therefore they were not treated quantitatively. As evaluation it

may be noticed that the cracks in {110} planes and big cracks in planes {100} are almost similar by size (judging by the maxima half-width), but the quantity of cracks in {110} is lower by several orders of value. They are able to form either by the mechanism of opening parallel slip planes that is possible under large loadings and high degrees of deformation [16] where high dislocation density occurs in the slipband and the distance between bands is small, or by Stroh mechanism (crack opening at the vertex of a dislocation cluster hindered by a tough detainer). In this case the dislocation cluster near the hindrance transform the dislocations near the detainer into cleaving ones [16], and the crystal cleavage and the crack formation result in some relaxation of the local stress and allow to the source to form new dislocation loops absorbed by the growing crack. The first mechanism under our conditions is not excluded but seems significantly less probable (because of small loading) than Stroh mechanism [16].

5. Conclusions

As a result of the experiments, their analysis and evaluations it was established that under cyclic loading of NaCl samples with relatively low loadings ($\simeq 10^7$ N/m^2), microscopic cracks occurred in them: small $k_a\tilde{a} < 1$ and big $k_a\tilde{a} \geq 1$, which are positioned at {100} planes and generated by Cottrell mechanism. Their volume fraction ($N\upsilon$) increases during the loading cycling. The critical size of the cracks estimated based on Griffith criterion including the factor of stress concentration agreed practically with the experimentally observed size of the formed small cracks.

In the late stages of deformation, the transformation of geometry of the crack assemble was found; this consisted in formation of ordered compact crack groups that was revealed by the peak splitting in diagrams $I(\varphi)$.

Along with cracks lying in {100} planes, in the late deformation stages the formation of the cracks lying in {110} planes was found. From two possible mechanisms of their formation (the mechanism of opening the parallel slip bands, and Stroh mechanism — the crack opening at the vertex of dislocation cluster hindered by tough detent), under our conditions with low loading and small deformation, Stroh mechanism is considered the most probable.

The volume fraction of small cracks exceeds by two orders of value the volume fraction of big cracks. The volume fractions of both kinds of the cracks increase with the cycle number, but the fraction of big cracks increases faster (more than by an order). Therefore, as to the risk of the crystal destruction, it is caused, first of all, by big cracks, not only due to fast increasing their total volume, but also in connection with the trend to formation of large ordered groups and, possibly the main (destroying) cracks.

References

1. G.A.Malygin, *Fiz.Tverdogo Tela*, **49**, 961 (2007).
2. A.M.Leksovskiy, B.L.Baskin, *Fiz.Tverdogo Tela*, **53**, 1157 (2011).
3. G.A.Malygin, *Fiz.Tverdogo Tela*, **51**, 1709 (2009).
4. L.B.Zuyev, V.I.Danilov, *Fiz.Tverdogo Tela*, **39**, 1399 (1997).
5. M.A.Lebedkin, L.P.Dunin-Barkovskiy, *Zh. Eksp. Teor. Fiz.*, **113**, 1816 (1998).
6. G.A.Malygin, *Fiz.Tverdogo Tela*, **44**, 1979 (2002).
7. V.R.Regel, A.I.Slutsker, E.Ye.Tomashevskiy, Kinetic Nature of Strength in Solids, Nauka, Moscow (1974) [in Russian].
8. Yu.I.Golovin, A.I.Tyurin, *Fiz.Tverdogo Tela*, **42**, 1818 (2000).
9. G.A.Malygin, *Uspehi Fiz. Nauk*, **169**, 979 (1999).
10. G.F.Sarafanov, *Fiz.Tverdogo Tela*, **50**, 1793 (2008).
11. V.G.Kononenko, D.V.Pluzhnikova, *Optika i Spektroskopia*, **50**, 489 (1981).
12. H.C.van de Hulst, Light Scattering by Small Particles, John Wiley & Sons, New York, Inc. Chapman & Hall. Ltd, London, (1957).
13. V.N.Betekhtin, A.G.Kadomtsev, *Fiz.Tverdogo Tela*, **47**, 801 (2005).
14. V.I.Smirnov, *Fiz.Tverdogo Tela*, **36**, 2037 (1994).
15. O.M.Savenko, G.I.Gering, *Fiz.Tverdogo Tela*, **34**, 11 (1992).
16. J.Hirth, J.Lothe, Theory of Dislocations, McGraw-Hill, New York (1968).
17. S.P.Timoshenko, J.Gudier, Theory of Elasticity, Nauka, Moscow (1975) [in Russian].
18. Ya.E.Geguzin, V.G.Kononenko, *FizKhom*, **1**, 131 (1981).
19. V.G.Kononenko, V.Khayler, *Kristallografia*, **25**, 765 (1980).
20. L.E.Kar'kina, O.A.Elkina, L.I.Yakovenkova, *Fiz.Tverdogo Tela*, **49**, 1063 (2007).

Механізми утворення і геометрія ансамблю тріщин, які формуються при одноосьовому циклічному стисканні монокристалів NaCl

Ю.І.Бойко, М.А.Волосюк, В.Г.Кононенко

Експериментально досліджено методом світлорозсіювання утворення тріщин у монокристалах NaCl в умовах одноосьового циклічного стискання (10^7 Н/м^2) протягом ~10 с при кімнатній температурі і подальшого відпалу при T = 500°С протягом 10 хв. Спостережувані тріщини за розмірами розділені (умовно, у порівнянні з довжиною хвилі світла, що використано) на малі, що дають ізотропну картину розсіювання, і великі, картина розсіювання світла якими містить різкі максимуми. Встановлено, що і малі, і великі тріщини розташовуються у площинах типу {100} і утворюються механізмом Коттрелла. На далеких стадіях деформування спостерігаються у невеликій кількості тріщини у площинах типу {110}. З можливих механізмів їх утворення у нашому випадку (малих деформацій і напружень) найбільш імовірним видається механізм Стро. Виявлено, у міру накопичення тріщин, утворення впорядкованих компактних груп тріщин, аналогічних упорядкованим групам твердих іншофазних виділень при розпаді пересичених твердих розчинів. Об'ємна частка малих тріщин на два порядки перевершує об'ємну частку великих. Об'ємні частки тих і інших зростають з номером циклу, але випереджальним темпом зростає частка великих тріщин.